Bayesian Inference Based Parameter Calibration of a Mechanical Load-Bearing Structure's Mathematical Model

Christopher M. Gehb[1,*] Roland Platz[1] and Tobias Melz[1,2]

[1] Technische Universität Darmstadt, System Reliability, Adaptive Structures and Machine Acoustics SAM, Magdalenenstraße 4, 64289 Darmstadt, Germany
[2] Fraunhofer Institute for Structural Durability and System Reliability LBF, Bartningstraße 47, 64289 Darmstadt, Germany
*gehb@sam.tu-darmstadst.de

ABSTRACT

Load-bearing structures with kinematic functions like a suspension of a vehicle and an aircraft landing gear enable and disable degrees of freedom and are part of many mechanical engineering applications. In most cases, the load path going through the load-bearing structure is predetermined in the design phase. However, if parts of the load-bearing structure become weak or suffer damage, e.g. due to deterioration or overload, the load capacity may become lower than designed. In that case, load redistribution can be an option to adjust the load path and, thus, reduce the effects of damage or prevent further damage. For an adequate numerical prediction of the load redistribution capability, an adequate mathematical model with calibrated model parameters is needed. Therefore, the adequacy of an exemplary load-bearing structure's mathematical model is evaluated and its predictability is increased by model parameter uncertainty quantification and reduction. The mathematical model consists of a mechanical part, a friction model and the electromagnetic actuator to achieve load redistribution, whereby the mechanical part is chosen for calibration in this paper. Conventionally, optimization algorithms are used to calibrate the model parameters deterministically. In this paper, the model parameter calibration is formulated to achieve a model prediction that is statistically consistent with the data gained from an experimental test setup of the exemplary load-bearing structure. Using the R^2 sensitivity analysis, the most influential parameters for the model prediction of interest, i.e. the load path going through the load-bearing structure represented by the support reaction forces, are identified for calibration. Subsequently, Bayesian inference based calibration procedure using the experimental data and the selected model parameters is performed. Thus, the mathematical model is adjusted to the actual operating conditions of the experimental load-bearing structure via the model parameters and the model prediction accuracy is increased. Uncertainty represented by originally large model parameter ranges can be reduced and quantified.

Keywords: adaptive systems, uncertainty quantification, Bayesian inference, parameter calibration

1 INTRODUCTION

Withstanding and distributing loads is often one of the key tasks in mechanical engineering applications such as load-bearing systems. Additionally, defined kinematics are also part of the functional performance in load-bearing systems with a specified movement of structural components. Typically, the load is transmitted from one or more transmission points through a predetermined load path to the structural supports. An example is the compression stroke of a landing gear or suspension strut in airplanes or vehicles. For this example, the load is distributed towards the structure's supports as predetermined and, mostly, not subject to any change during the structure's lifetime. However, if properties, e.g. damping and stiffness or strength of the supports are uncertain or vary over time, load redistribution to bypass portions of loading away from for example weakened structural components could be an option to prevent the structure from failure or reduced comfort [1–3]. For an adequate numerical prediction of the dynamic behavior of such a structure, an adequate mathematical model with calibrated model parameters is needed.

In particular, the load path represented by the support reaction forces is of interest in this paper. The demands regarding the reduction of model prediction uncertainty increase since model predictions are used for controller tuning, system design and decision making [4–6]. Uncertainty quantification and reduction in model predictions help to achieve a reliable and adequate model prediction. Reducing the model prediction uncertainty is achieved i.a. via calibrating the mathematical model's parameters [7–9]. Thus, the mathematical model is adjusted to the experimentally observed dynamic behavior.

Parameter calibration is commonly achieved by solving an optimization problem to find deterministic values for each model parameter to be calibrated that best fit the chosen calibration criteria. For example in [10], parameters of a friction model were identified for a direct-drive rotary torque motor using the Novel Evolutionary Algorithm optimization. Experimental data from a test rig was used within the optimization process and two objective functions were minimized for different parameter sets. As a result, the calibrated parameters are stated as deterministic values. Similar procedures but using for example genetic and particle swarm optimization algorithms for model parameter calibration can be found in [8] and [11] for models of mechanical servo systems. In these studies, uncertainty in calibrated parameters as remaining parameter variabilities were not taken into account. Hence, deterministic optimization approaches are searching for the best fitting parameter values and then treating the parameters as known and fixed. In contrast, non-deterministic calibration approaches aim to achieve statistical consistency between model output and experimental data [12, 13]. In [14] the model parameters of a historic masonry monument FE model have been calibrated using a non-deterministic calibration approach. The Bayesian inference with Markov Chain Monte Carlo leads to calibrated model parameters with resulting reduced model prediction uncertainty. The same approach was used in a two-part paper [9, 15] to calibrate the model parameters of a wind turbine blade FE model. It was possible to find a simplified but still credible model by reducing the prediction uncertainty applying verification and validation methods. Another example for statistical parameter calibration can be found in [7]. Bayesian inference was successfully used to calibrate parameters for several friction models, but inconclusive for the LuGre-model parameters. A possible reason was the little effect of some LuGre-parameters on the experimentally measured features that made adequate calibration impossible. Successfully use of Bayesian inference for LuGre-model parameters calibration was conducted in [16]. In non-deterministic calibration approaches, the calibrated model parameters are stated as distributions representing the remaining parameter uncertainty [12].

In this paper, the model parameters of a load-bearing structure that enables load redistribution with semi-active guidance elements, [2] and [3], are calibrated using the non-deterministic Bayesian inference uncertainty quantification and preceding sensitivity analysis [12, 15]. The complete mathematical model is divided into two parts, a part representing the mechanics of the load-bearing structure, in the following referred to load-bearing structure, and a part representing the semi-active guidance elements with friction phenomena and the electromagnetic actuator to operate the friction brake. The model parameters of semi-active guidance elements are not in the scope of this work but have already been calibrated in the aforementioned paper [16] and also in [13]. Here, the model parameters of the load-bearing structure's model are of interest. Experimental data used for the load-bearing structure's model parameter calibration is measured from a test rig with step excitation. The non-deterministic Bayesian inference statistically correlates the model predictions with the measurements. Additionally, it enables to quantify and reduce model parameter uncertainty concurrently and increases prediction accuracy since parameters and model predictions are not assumed as deterministic and, hence, better represent the typically non-deterministic reality. Therefore, the non-deterministic Bayesian inference is preferred to a deterministic calibration approach. The load-bearing structure and its corresponding mathematical model are introduced in Sec. 2. The model calibration procedure including sensitivity analysis and Bayesian inference is performed in Sec. 3. In Sec. 4, the comparison of model predictions with non-calibrated and calibrated model parameters are presented. Finally, conclusions and proposed future work are given in Sec. 5.

2 LOAD-BEARING STRUCTURE UNDER INVESTIGATION

The investigated load-bearing structure is derived from a complex load-bearing system that has been developed in the German Collaborative Research Center (German acronym SFB) 805 "Control of Uncertainty in Load-Carrying Structures in Mechanical Engineering" at the Technische Universität Darmstadt. This load-bearing system is a Modular Active Spring Damper System (German acronym MAFDS) and serves as an example for a modular structure with passive, semi-active and active modules to study uncertainty in different approaches to control stability and

vibration as well as adapt load paths [17, 18]. The derived load-bearing structure in the scope of this paper consists of a translational moving mass m_A connected to a rigid beam with mass m_B and mass moment of inertia Θ_B by a spring-damper with stiffness k_S and damping coefficient b_S and two kinematic guidance elements as depicted in Fig. 1. Two supports at the ends of the beam are equipped with adjustable stiffnesses to simulate weakened structural components when stiffness is reduced. A weakened or damaged structural component is assumed to be one of the two supports and is represented by a reduced support stiffness representing reduced load capacity. The semi-active load redistribution can be used to relieve the weak structural components, monitoring the load path via the support reaction forces [1–3].

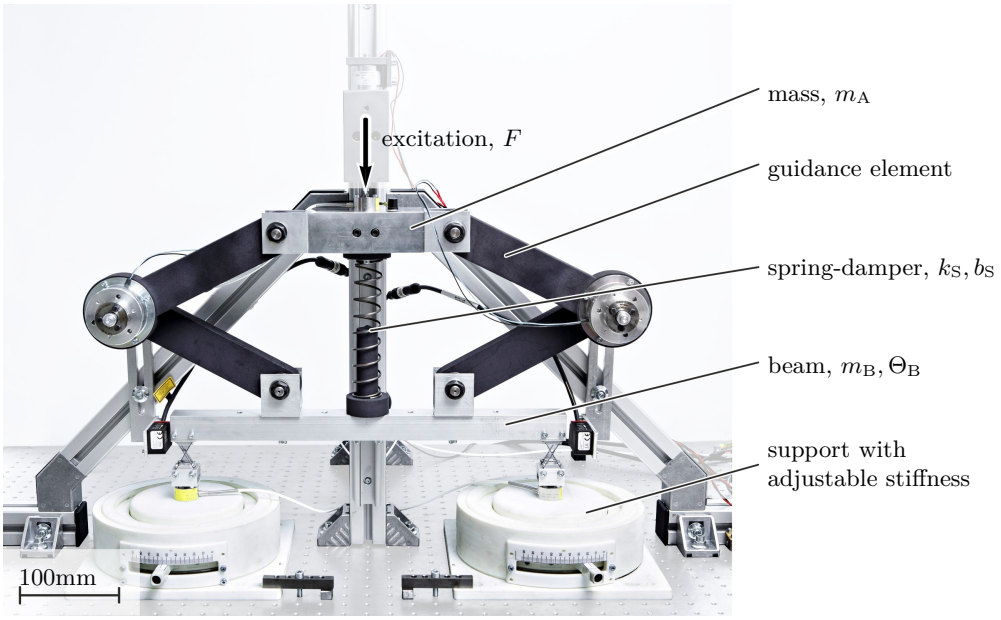

Fig. 1 Exemplary load-bearing structure with semi-active guidance elements for load redistribution and adjustable supports to simulate weak or damaged support conditions [13]

2.1 MATHEMATICAL MODEL OF THE LOAD-BEARING STRUCTURE

Fig. 2 depicts the mechanical model and the free body diagram of the load-bearing structure. Three independent degrees of freedom (DOF) that are the vertical displacements in z_A- and z_B-direction and the rotation in φ-direction are introduced, Fig. 2(a). The mechanical model consists of a movable mass m_A, a rigid beam with mass m_B, with mass moment of inertia Θ_B in x-z-plane and length l_B. The associated DOF are z_A, z_B and φ. The masses m_A and m_B are symmetrically connected to each other by two semi-active guidance elements, one on each side of the beam. The semi-active guidance elements are connected to the beam at the contact points $x = a$ and $x = l_\mathrm{B} - a$. Additionally, a spring-damper system with stiffness and damping coefficients k_S and b_S connects the mass m_A and the beam at $x = l_\mathrm{B}/2$. The beam is connected to the ground at $x = 0$ and $x = l_\mathrm{B}$ via two elastic supports L and R with stiffnesses k_L and k_R and viscous damping coefficients b_L and b_R shown in Fig. 2(b) [2, 3, 13].

According to [13], the linear time-dependent support displacements in Fig. 2(a)

$$z_\mathrm{L} = -\varphi \frac{l_\mathrm{B}}{2} + z_\mathrm{B} \qquad \text{and} \qquad z_\mathrm{R} = \varphi \frac{l_\mathrm{B}}{2} + z_\mathrm{B} \tag{1}$$

result from the two DOF z_B and φ related to the beam assuming small beam angles φ with $\sin\varphi \approx \varphi$. The support displacement difference $z_\mathrm{R} - z_\mathrm{L}$ represents the beam's misalignment. The linear time dependent displacements

$$z_\mathrm{ge,L} = -\varphi \left(\frac{l_\mathrm{B}}{2} - a \right) + z_\mathrm{B} \qquad \text{and} \qquad z_\mathrm{ge,R} = \varphi \left(\frac{l_\mathrm{B}}{2} + a \right) + z_\mathrm{B} \tag{2}$$

are the beam displacement at the semi-active guidance element connection points again assuming small beam angles φ with $\sin\varphi \approx \varphi$. According to Fig. 2(b), the internal spring and damping forces of the spring-damper system are

$$F_{\mathrm{k,S}} = k_{\mathrm{S}}\,(z_{\mathrm{B}} - z_{\mathrm{A}})\,, \tag{3a}$$
$$F_{\mathrm{b,S}} = b_{\mathrm{S}}\,(\dot{z}_{\mathrm{B}} - \dot{z}_{\mathrm{A}}) + F_{\delta} \tag{3b}$$

with the dissipative force caused by inherent friction

$$F_{\delta} = F_{\mu} \tanh\left(\frac{(\dot{z}_{\mathrm{B}} - \dot{z}_{\mathrm{A}})}{v_0}\right). \tag{4}$$

The tanh function in (4) causes a constant change of the friction induced force F_{μ} at the zero-crossing of $(\dot{z}_{\mathrm{B}} - \dot{z}_{\mathrm{A}})$ to yield the dissipative force F_{δ} and avoids numerical issues associated with Coulomb friction such as model discontinuity [19]. The constant velocity v_0 defines the slope of the tanh function and is arbitrary except for $v_0 < v_{\mathrm{S}}$ with the Stribeck velocity v_{S} [19, 20].

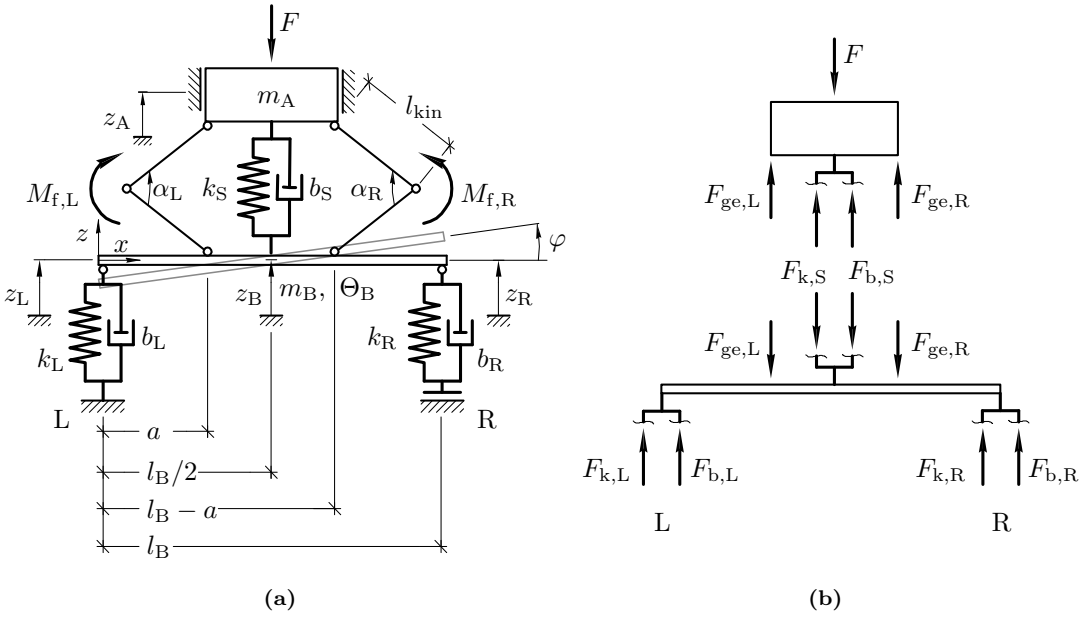

(a) **(b)**

Fig. 2 Mechanical model of the load-bearing structure, **(a)** degrees of freedom and relevant model parameters and **(b)** free body diagram with internal and external forces [13]

The internal spring and damping forces of the supports L and R are

$$F_{\mathrm{k,L}} = -k_{\mathrm{L}}\, z_{\mathrm{L}} \qquad \text{and} \qquad F_{\mathrm{b,L}} = -b_{\mathrm{L}}\, \dot{z}_{\mathrm{L}} \tag{5a}$$
$$F_{\mathrm{k,R}} = -k_{\mathrm{R}}\, z_{\mathrm{R}} \qquad \text{and} \qquad F_{\mathrm{b,R}} = -b_{\mathrm{R}}\, \dot{z}_{\mathrm{R}}. \tag{5b}$$

The combined support reaction and spring-damper system forces are

$$F_{\mathrm{L}} = F_{\mathrm{k,L}} + F_{\mathrm{b,L}}, \tag{6a}$$
$$F_{\mathrm{R}} = F_{\mathrm{k,R}} + F_{\mathrm{b,R}}, \tag{6b}$$
$$F_{\mathrm{S}} = F_{\mathrm{k,S}} + F_{\mathrm{b,S}}. \tag{6c}$$

The excitation force applied to the mass m_{A}

$$F(t) = \begin{cases} 0 & \text{for } t < t_{\mathrm{exc}}, \\ \widehat{F} & \text{for } t \geq t_{\mathrm{exc}} \end{cases} \tag{7}$$

is assumed as a step-function with the time of excitation t_{exc} caused by the release of a load mass. When assuming load redistribution, the semi-active guidance elements provide additional moments $M_{\mathrm{f,L}}$ and $M_{\mathrm{f,R}}$, Fig. 2(a), to

achieve the desired load redistribution. $M_{\mathrm{f,L}}$ and $M_{\mathrm{f,R}}$ result in vertical guidance element forces $F_{\mathrm{ge,L}}$ and $F_{\mathrm{ge,R}}$ that directly act on the mass m_{A} and the connection points at $x = a$ and $x = l_{\mathrm{B}} - a$ on the beam and are responsible for the load redistribution, Fig. 2(b). However, the semi-active load redistribution is not addressed in this paper, details to control and model parameter calibration of the semi-active guidance elements can be found in [3, 13, 16].

According to the direction of internal forces in (3) and (5) and Fig. 2(b), the linear equation of motion system of the load-bearing structure becomes

$$\begin{aligned}
&\underbrace{\begin{bmatrix} m_{\mathrm{A}} & 0 & 0 \\ 0 & m_{\mathrm{B}} & 0 \\ 0 & 0 & \Theta_{\mathrm{B}} \end{bmatrix}}_{\boldsymbol{M}} \underbrace{\begin{bmatrix} \ddot{z}_{\mathrm{A}} \\ \ddot{z}_{\mathrm{B}} \\ \ddot{\varphi} \end{bmatrix}}_{\ddot{\boldsymbol{r}}} + \underbrace{\begin{bmatrix} b_{\mathrm{S}} & -b_{\mathrm{S}} & 0 \\ -b_{\mathrm{S}} & b_{\mathrm{S}}+b_{\mathrm{L}}+b_{\mathrm{R}} & -\frac{l_{\mathrm{B}}}{2} b_{\mathrm{L}}+\frac{l_{\mathrm{B}}}{2} b_{\mathrm{R}} \\ 0 & -\frac{l_{\mathrm{B}}}{2} b_{\mathrm{L}}+\frac{l_{\mathrm{B}}}{2} b_{\mathrm{R}} & \frac{l_{\mathrm{B}}^2}{4} b_{\mathrm{L}}+\frac{l_{\mathrm{B}}^2}{4} b_{\mathrm{R}} \end{bmatrix}}_{\boldsymbol{D}} \underbrace{\begin{bmatrix} \dot{z}_{\mathrm{A}} \\ \dot{z}_{\mathrm{B}} \\ \dot{\varphi} \end{bmatrix}}_{\dot{\boldsymbol{r}}} + \ldots \\
&\underbrace{\begin{bmatrix} k_{\mathrm{S}} & -k_{\mathrm{S}} & 0 \\ -k_{\mathrm{S}} & k_{\mathrm{S}}+k_{\mathrm{L}}+k_{\mathrm{R}} & -\frac{l_{\mathrm{B}}}{2} k_{\mathrm{L}}+\frac{l_{\mathrm{B}}}{2} k_{\mathrm{R}} \\ 0 & -\frac{l_{\mathrm{B}}}{2} k_{\mathrm{L}}+\frac{l_{\mathrm{B}}}{2} k_{\mathrm{R}} & \frac{l_{\mathrm{B}}^2}{4} k_{\mathrm{L}}+\frac{l_{\mathrm{B}}^2}{4} k_{\mathrm{R}} \end{bmatrix}}_{\boldsymbol{K}} \underbrace{\begin{bmatrix} z_{\mathrm{A}} \\ z_{\mathrm{B}} \\ \varphi \end{bmatrix}}_{\boldsymbol{r}} = \underbrace{\begin{bmatrix} -F + F_\delta + F_{\mathrm{ge,L}} + F_{\mathrm{ge,R}} \\ -F_\delta - F_{\mathrm{ge,L}} - F_{\mathrm{ge,R}} \\ (\frac{l_{\mathrm{B}}}{2} - a)\, F_{\mathrm{ge,L}} - (\frac{l_{\mathrm{B}}}{2} - a)\, F_{\mathrm{ge,R}} \end{bmatrix}}_{\boldsymbol{F}}
\end{aligned} \tag{8}$$

for translational z_{A}- and z_{B}-directions as well as for rotational φ-direction. In Eq. (8), $\boldsymbol{M}$, $\boldsymbol{D}$ and $\boldsymbol{K}$ are the [3×3] mass, damping and stiffness matrices, and $\ddot{\boldsymbol{r}}$, $\dot{\boldsymbol{r}}$ and $\boldsymbol{r}$ are the [3×1] translational and angular acceleration, velocity and displacement vectors. The [3×1] force vector $\boldsymbol{F}$ contains the excitation force F (7) acting on the mass m_{A}, the dissipative force F_δ (4) as well as the forces $F_{\mathrm{ge,L}}$ and $F_{\mathrm{ge,R}}$ for load redistribution and provided by the semi-active guidance elements in Fig. 2(b). In the scope of this paper, $F_{\mathrm{ge,L}} = F_{\mathrm{ge,R}} = 0$ since the semi-active load redistribution control is not further investigated.

The mathematical model of the load-bearing structure is derived to capture the load path through the structure and to predict and assess the load redistribution capability in case of the semi-active structure in [3, 13, 16]. In particular, the mathematical model predictions include the misalignment of the beam φ that is defined as malfunction and the support reaction forces F_{R} and F_{L} as measures for the load path. This paper focuses the calibration of the load-bearing structure's model parameters, see Sec. 2.2.

The derived mathematical model (1) to (8) underlies the following model simplifications. Undesired friction occurring in joints, parallel guidance rails and supports is simplified and summarized to a single dissipative force F_δ in (4) with the related model parameter F_μ. The assumption of lumped masses and rigid bodies leads to neglected structural elasticities of the components, compare Fig. 2(b). The structural elasticities of the components are significantly larger than the considered elasticities of the spring and supports and, hence, do not contribute to the relevant dynamic behavior for load redistribution. Although the simplified load-bearing structure is assumed to be planar, the experimental test setup, compare Fig. 1, is inevitable spatial. However, this has only little to no effect for the relevant z-direction. The spring-damper system and the guidance elements are assumed to be free of mass. Their mass contributions are allocated to the masses m_{A} and m_{B} [13]. These model simplifications might contribute to parameter uncertainty and can be considered via parameter calibration, see Sec. 2.2 and Sec. 3.

2.2 MODEL PARAMETERS

Tab. 1 introduces all model parameters needed to simulate the dynamic behavior of the load-bearing structure's mathematical model (8). The most influential model parameters that need to be calibrated must be selected based upon both their uncertainty and sensitivity on the model predictions of interest. The parameter uncertainty might result from missing manufacturer information, non-measurable model parameters resulting from simplifications or empirical models with non-physical parameters [13, 21, 22]. With knowledge regarding the previously described uncertainty sources and a subsequent sensitivity analysis, Sec. 3.1, the most influential calibration parameters can be identified. Model parameters such as k_{L} and k_{R} related to the adjustable supports are not calibrated since they can be measured and are also investigated more detailed in [13]. The beam length l_{B} can also be measured and the

stiffness coefficient k_S is given by the manufacturer. Thus, the uncertainty of these parameters is assumed to be small compared to other model parameters in Tab. 1 and they are kept constant and are not subject for parameter calibration. The beam's mass moment of inertia Θ_B directly results from the beam's cross section geometry and its mass m_B and, therefore, is no individual calibration candidate.

Tab. 1 Model parameters of the load-bearing structure, parameters with stated values are not subject for calibration, calibration candidate parameters are referenced to Tab. 2 and Tab. 3 [13]

property	symbol	value	unit
support properties			
stiffness support left	k_L	30,000	N/m
stiffness support right	k_R	30,000	N/m
structure properties			
upper mass A	m_A	Tab. 3	kg
beam mass B	m_B	Tab. 2	kg
beam mass moment of inertia	Θ_B	0.0417	$\mathrm{kg\,m^2}$
viscous damping coefficient	b_S	Tab. 3	Ns/m
friction damping	F_μ	Tab. 3	N
stiffness coefficient	k_S	1440	N/m
beam length	l_B	0.4	m

The damping related model parameters F_μ and b_S are typically uncertain parameters and not determined without experiments [23]. Technically, the masses m_A and m_B are measurable. Since the guidance elements are assumed to be free of mass, it is reasonable to allot their amount of mass to the masses m_A and m_B. Hence, the model parameters m_A and m_B are influenced by model simplifications with resulting increased uncertainty. Summing up, the model parameters F_μ, b_S, m_A and m_B are identified as potential calibration candidates due to their uncertainty. Model parameters with negligible uncertainty or sensitivity will not be calibrated to reduce the computational effort. The sensitivity for the model parameters summarized in the calibration candidate vector $\boldsymbol{\theta} = [F_\mu, b_S, m_A, m_B]$ is assessed in Sec. 3.1.

3 MODEL PARAMETER CALIBRATION PROCEDURE

The sensitivities of the damping related model parameters F_μ and b_S as well as the masses m_A and m_B upon a comparative feature are calculated, see Sec. 3. A comparative feature represents a relevant output of the mathematical model or unambiguous physical properties and states to which the model is calibrate to [13, 14, 24]. The experimental and numerical outputs of interest for the model parameter calibration of the load-bearing structure are the support reaction forces F_L and F_R (6) representing the load path through the load-bearing structure. The comparative feature to calibrate the load-bearing structure is assumed to be

$$Y^{M/E}(t, \boldsymbol{\theta}) = \frac{1}{2}\left(F_L(t) + F_R(t)\right), \tag{9}$$

representing the time-history of the average support reaction force obtained from the mathematical model predictions Y^M or the experimental results Y^E for the step excitation in (7) and a time record from $t = 0\,\mathrm{s}$ to $t = 2\,\mathrm{s}$. In case of equal support stiffness of the left and right support $k_L = k_R$, the numerically calculated support reaction forces are equal, as the experimental results. Hence, there is no need to calibrate both sides individually and the average support reaction force is chosen as comparative feature. The measured support reaction forces F_L and F_R to calibrate the model parameters of the load-bearing structure are obtained from the experimental test setup introduced in Fig. 1.

3.1 SENSITIVITY ANALYSIS

The sensitivity of the mathematical model predictions on parameter variations is assessed by calculating the statistical significance of parameter variations on the model prediction variation. Thus, the influence of the model parameters

with respect to the comparative features Y^{M} (9) is identified. The assessment of the statistical significance is carried out with an analysis of variance (ANOVA) using the coefficient of determination R^2 [14, 25].

The coefficient of determination

$$\mathrm{R}_\theta^2 = \left(1 - \frac{\mathrm{SSE}_\theta}{\mathrm{SST}}\right) \cdot 100\,\% \tag{10}$$

calculates the proportion of model output variability that can be ascribed to each calibration candidate parameters variation. The *sum of squares total* (SST) is the total model variability and the *sum of squares error* (SSE) is the unexplained model variability of the calibration candidate parameters $\boldsymbol{\theta}$. More details regarding SST and SSE can be found in [13, 14, 25, 26]. The results for each calibration candidate parameter are between $0\,\% \leq \mathrm{R}_\theta^2 \leq 100\,\%$. High R^2 values are used to identify the most influential parameters. The results are typically summarized in tables and a threshold is chosen that defines the minimum R^2 value for being a calibration candidate. By first using the sensitivity analysis, ill-conditioning can be prevented and computational burden reduced if only the most influential parameters are selected to be calibrated [14].

The R^2 (10) sensitivity analysis results are listed in Tab. 2 for each calibration candidate parameter, averaged over the simulation time $t = 0\,\mathrm{s}$ to $t = 2\,\mathrm{s}$ since the comparative feature $Y^{\mathrm{M}}(t, \boldsymbol{\theta})$ (9) is time dependent. The lower bounds for the mass m_{A} and the beam mass m_{B} are their measured weights. The upper bounds are chosen with additional $2\,\mathrm{kg}$ considering the potential mass of the assumed to be free mass guidance elements. The upper and lower bounds for b_{S} and F_μ are best guesses, which result from preliminary numerical tests. A significant proportion of variability of Y^{M} with 73.04% is explained by the mass m_{A}. Another 7.68% and 19.20% of variability are explained by the viscous damping coefficient b_{S} and the friction damping F_μ. Thus, these parameters are calibrated with experimental data. The beam mass m_{B} contributes less than 1% to the variability of Y^{M} and is not calibrated with experimental data [13].

Tab. 2 R^2 statistics for the calibration candidate parameters and the parameter bounds for the sensitivity analysis of the load-bearing structure, R^2 values are scaled to 100 % [13]

parameter	lower bound	upper bound	R^2	calibrate?
m_{A}	$1.4\,\mathrm{kg}$	$3.4\,\mathrm{kg}$	73.04 %	Yes
m_{B}	$0.25\,\mathrm{kg}$	$2.25\,\mathrm{kg}$	0.17 %	No
b_{S}	$5.0\,\mathrm{N\,s\,m^{-1}}$	$10.0\,\mathrm{N\,s\,m^{-1}}$	7.68 %	Yes
F_μ	$0.8\,\mathrm{N}$	$1.6\,\mathrm{N}$	19.20 %	Yes

Only parameter with significant influence on the output variability ($\mathrm{R}^2 < 1\%$) are taken into account for the following calibration process. The calibration parameters are, again, summarized in the calibration parameter vector $\boldsymbol{\theta} = [m_{\mathrm{A}}, b_{\mathrm{S}}, F_\mu]$ and are reduced from 9 model parameters in Tab. 1 to 3 calibration parameters to be calibrated via Bayesian inference, see Tab. 2.

3.2 BAYESIAN INFERENCE FOR MODEL PARAMETER CALIBRATION

Bayesian inference is used as statistical calibration approach to calibrate uncertain model parameters identified in Sec. 3.1. The aim of statistical uncertainty inference is to statistically correlate the model predictions with the measurements by solving an inverse problem [27]. The relation between measurements and simulations according to [12, 28, 29] is given by

$$Y_n^{\mathrm{E}}(t) = Y_n^{\mathrm{M}}(t, \boldsymbol{\theta}) + \varepsilon_n(t),\ n = 1, ..., N \tag{11}$$

where $Y_n^{\mathrm{E}}(t)$ represents the experimentally measured comparative feature and N is the number of measurements. The numerically predicted comparative feature $Y_n^{\mathrm{M}}(t, \boldsymbol{\theta})$ is supplemented by the measurement error $\varepsilon_n(t) \sim \mathcal{N}(0, \sigma^2)$, that is assumed to be independent and identically distributed (iid) and normally distributed with zero mean and standard deviation σ [28]. The Bayesian inference approach statistically connects the simulation outputs Y^{M} as

hypothesis and the measurement outputs Y^{E} by taking into account the hypothesis and measurement probability to adequately calibrate varied model parameters $\boldsymbol{\theta}$. Current knowledge of the system and its model parameters is updated with new information obtained from experimental tests. Thus, the parameter uncertainty is reduced and quantified by systematic inference of the posterior distribution [28, 29]. Using the Bayes' Theorem [28, 30], the posterior parameter distribution given the experimental results can be stated as

$$P(\boldsymbol{\theta}, Y^{\mathrm{M}}|Y^{\mathrm{E}}) = \frac{L(Y^{\mathrm{E}}|\boldsymbol{\theta}, Y^{\mathrm{M}}) \times P(\boldsymbol{\theta})}{P(Y^{\mathrm{E}})} \tag{12}$$

with the likelihood function $L(Y^{\mathrm{E}}|\boldsymbol{\theta}, Y^{\mathrm{M}})$ representing the probability of experimental outputs Y^{E} given a set of parameters $\boldsymbol{\theta}$ for the mathematical model output Y^{M} [13, 28]. If no further information regarding the prior distribution $P(\boldsymbol{\theta})$ in Eq. (12) is available, a uniform distribution between certain upper and lower bounds is assumed.

Because the denominator $P(Y^{\mathrm{E}})$ in Eq. (12), the total probability or evidence, is typically not computable with reasonable effort and is only normalizing the result anyway [7], it is more practical to sample from a proportional relationship of the posterior parameter distribution

$$P(\boldsymbol{\theta}, Y^{\mathrm{M}}|Y^{\mathrm{E}}) \propto L(Y^{\mathrm{E}}|\boldsymbol{\theta}, Y^{\mathrm{M}}) \times P(\boldsymbol{\theta}). \tag{13}$$

In this paper, the parameter space is explored using the Marcov Chain Monte Carlo (MCMC) sampling algorithm to approximate the posterior parameter distributions $P(\boldsymbol{\theta}, Y^{\mathrm{M}}|Y^{\mathrm{E}})$ by drawing multiple samples from these posterior parameter distributions. That is, the histograms of the calibration candidate parameters $\boldsymbol{\theta}$ of all random samples produce the approximated posterior parameter distributions $P(\boldsymbol{\theta}, Y^{\mathrm{M}}|Y^{\mathrm{E}})$ [28, 31]. By use of MCMC sampling, it is possible to eliminate the denominator $P(Y^{\mathrm{E}})$ in Eq. (12) and, thus, to enable a mathematical efficient application of Bayesian inference [28].

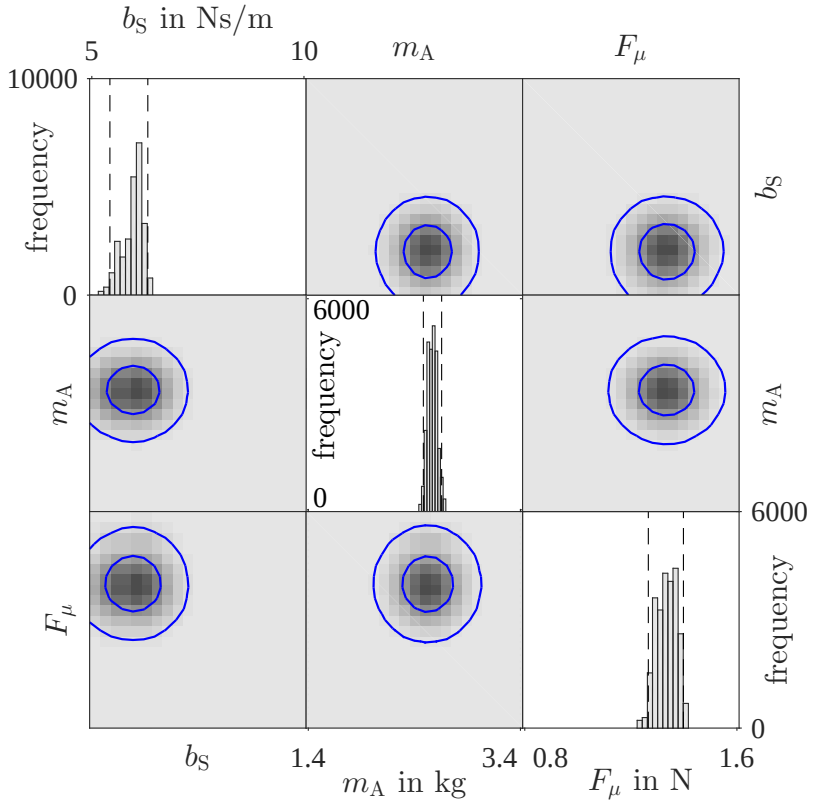

Fig. 3 Posterior distribution with 95% interpercentile intervals (– –) for the viscous damping b_{S}, the upper mass m_{A} and the friction induced force F_{μ} as result of the load-bearing structure calibration [13]

Fig. 3 depicts the parameter calibration results obtained from 25000 MCMC runs. On the diagonals, the parameter distributions are shown as histograms representing approximations of the posterior parameter distributions for the

three parameters $\boldsymbol{\theta} = [m_\mathrm{A}, b_\mathrm{S}, F_\mu]$. The off-diagonals depict distribution contour plots for the joint probability distribution pairs of the parameters. The modes of the calibrated parameters are $m_\mathrm{A} = 2.6\,\mathrm{kg}$, $b_\mathrm{S} = 6.1\,\mathrm{Ns\,m^{-1}}$ and $F_\mu = 1.35\,\mathrm{N}$. Furthermore, the narrow histograms graphically depict the knowledge gain and the uncertainty reduction for the parameter ranges. Tab. 3 summarizes the prior and posterior uncertainty in form of parameter bounds and the 95 % interpercentiles after parameter calibration [13]. The model parameter ranges covering the 95 % interpercentile can be reduced about 89 % for the mass m_A, about 82 % for the viscous damping b_S and about 84 % for the dissipative force F_μ compared to the prior bounds.

Tab. 3 Prior and posterior uncertainty in form of bounds and 95 % interpercentiles of the calibration parameters, uncertainty reduction from prior bounds to 95 % interpercentiles ranges [13]

	prior bounds		posterior 95 % interpercentile		
parameter	lower bound	upper bound	lower bound	upper bound	uncertainty reduction
m_A	$1.4\,\mathrm{kg}$	$3.4\,\mathrm{kg}$	$2.51\,\mathrm{kg}$	$2.73\,\mathrm{kg}$	89 %
b_S	$5.0\,\mathrm{Ns\,m^{-1}}$	$10.0\,\mathrm{Ns\,m^{-1}}$	$5.47\,\mathrm{Ns\,m^{-1}}$	$6.35\,\mathrm{Ns\,m^{-1}}$	82 %
F_μ	$0.8\,\mathrm{N}$	$1.6\,\mathrm{N}$	$1.26\,\mathrm{N}$	$1.39\,\mathrm{N}$	84 %

4 COMPARISON OF THE NON-CALIBRATED AND CALIBRATED MODEL PREDICTIONS

The effect of the statistical calibration procedure discussed in Sec. 3 on the model prediction accuracy is exemplarily shown in Fig. 4 providing non-calibrated ( ) and calibrated ( ) simulation results for a step load excitation $F = 25\,\mathrm{N}$ (7). The envelopes of each 300 MC simulation runs for non-calibrated and calibrated parameter ranges are conducted and compared to the related support reaction force measurements F_L (—) and F_R (—) averaged for 10 measurement repetitions. The non-calibrated model parameter ranges are equal distributed between the lower and upper prior bounds in Tab. 3. The calibrated model parameter ranges are distributed according to the histograms on the diagonal in Fig. 4 with the 95 % interpercentiles in Tab. 3.

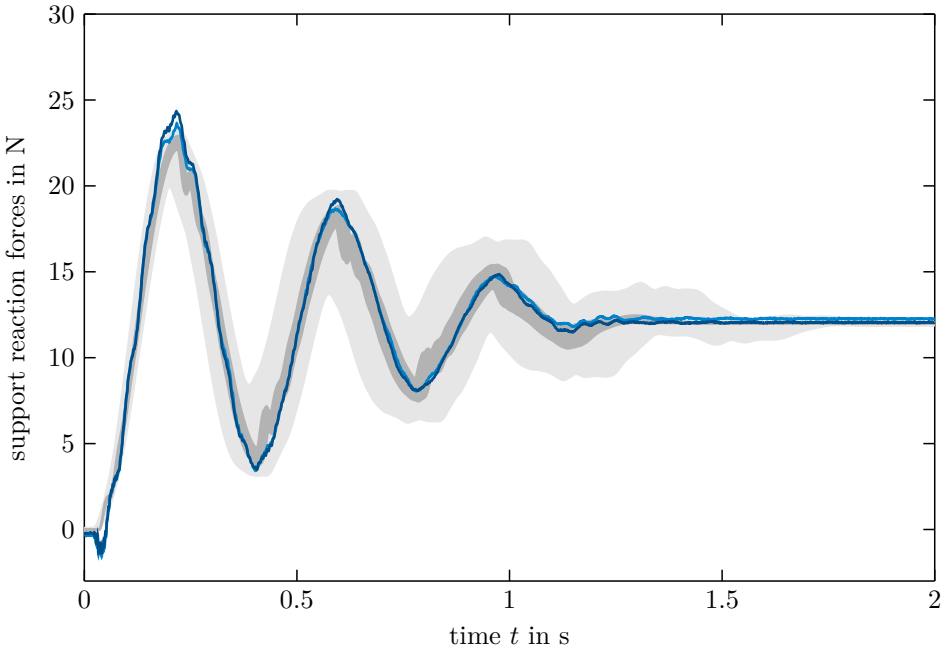

Fig. 4 Measured support reaction force F_L (—) and F_R (—) vs. time t and model predictions non-calibrated ( ) and calibrated ( ) applying step load excitation $F = 25\,\mathrm{N}$ (7) [13]

For the MC simulations in Fig. 4, the values of the model parameters, which are not selected for calibration, are chosen to be the mean value of the upper and lower bounds in Tab. 3 or to be deterministic according to Tab. 1 based on measurements or manufacturer information for the following numerical investigation via the MC simulation runs. The simulations using calibrated model parameters tend to be closer to the measurement with smaller envelopes. Even though calibrated and non-calibrated envelopes widely encompass the measurements for both supports, the envelope area of the calibrated MC simulations ( ) is significantly reduced by 75 % compared to the envelope area of the non-calibrated MC simulations ( ).

5 CONCLUSION

This paper presents a non-deterministic model parameter calibration approach for the load-bearing structure model to calculate the load path. The load-bearing structure is intended to investigate load redistribution via an alternative load path provided by semi-active guidance elements. The model parameters are calibrated to achieve model predictions that are statistically consistent with the experimental data. This means not to have a potentially over fitted deterministic value for each model parameter but a most likely values and related distributions representing the quantification of uncertainty. Model parameters with negligible uncertainty or sensitivity will not be calibrated to reduce the computational effort. Three model parameters turned out to be most influencing regarding the comparative feature taken into account. These are the viscous damping coefficient b_S, the friction damping F_μ and the mass m_A. With the reduced number of model parameters to be calibrated, the BAYESIAN inference is performed as statistical calibration approach. The size of the model parameter ranges, indicating the parameter uncertainty, can be reduced about 89 % for the mass m_A, about 82 % for the viscous damping b_S and about 84 % for the dissipative force F_μ compared to the prior distribution bounds selected during initialization of the calibration procedure. Overall, the model prediction distribution is reduced about 75 % comparing model predictions with non-calibrated and calibrated model parameters. Hence, by reducing the model parameter uncertainty, the model prediction accuracy can be increased. In future work, the calibrated model of the load-bearing structure will be used to improve the simulation results' accuracy of the semi-active system used to investigate semi-active load redistribution. Furthermore, the remaining model discrepancy after model parameter calibration may be used to identify missing physics or oversimplifications in the mathematical model.

ACKNOWLEDGEMENTS

The authors like to thank the Deutsche Forschungsgemeinschaft (DFG, German Research Foundation) for funding this project within the Sonderforschungsbereich (SFB, Collaborative Research Center) 805 "Control of Uncertainties in Load-Carrying Structures in Mechanical Engineering" – project number: 57157498.

REFERENCES

[1] Gehb, C. M., Platz, R., and Melz, T. "Active load path adaption in a simple kinematic load-bearing structure due to stiffness change in the structure's supports". In: *Journal of Physics: Conference Series* 744.1 (2016), p. 012168.

[2] Gehb, C. M., Platz, R., and Melz, T. "Global Load Path Adaption in a Simple Kinematic Load-Bearing Structure to Compensate Uncertainty of Misalignment Due to Changing Stiffness Conditions of the Structure's Supports". In: *Model Validation and Uncertainty Quantification, Volume 3*. Ed. by Barthorpe Robert J. et al. Conference proceedings of the Society for Experimental Mechanics series. Cham: Springer International Publishing, 2017, pp. 133–144.

[3] Gehb, C. M., Platz, R., and Melz, T. "Two control strategies for semi-active load path redistribution in a load-bearing structure". In: *Mechanical Systems and Signal Processing* 118 (2019), pp. 195–208.

[4] Herold, S., Jungblut, T., and Kurch, M. "A Systematic Approach to Simulate Active Mechanical Structures". In: *Multi-Disciplinary Simulations - The Future of Virtual Product Development*. 2009.

[5] Tamm, C. et al. “Methodisches Vorgehen zur Auslegung des vibro-akustischen Verhaltens eines Fahrzeugs”. In: *Smarte Strukturen und Systeme*. Ed. by Wiedemann, M., Misol, M., and Melz, T. Berlin, Boston: De Gruyter Oldenbourg, 2016, pp. 95–106.

[6] Platz, R. and Götz, B. “Non-probabilistic Uncertainty Evaluation in the Concept Phase for Airplane Landing Gear Design”. In: *Model Validation and Uncertainty Quantification, Volume 3*. Ed. by Barthorpe Robert J. et al. Conference proceedings of the Society for Experimental Mechanics series. Cham: Springer International Publishing, 2017.

[7] Green, P. L. and Worden, K. “Modelling Friction in a Nonlinear Dynamic System via Bayesian Inference”. In: *Special Topics in Structural Dynamics, Volume 6*. Ed. by Allemang, R. et al. New York, NY: Springer New York, 2013, pp. 543–553.

[8] Liu, D.-P. “Parameter Identification for LuGre Friction Model using Genetic Algorithms”. In: *Proceedings of 2006 International Conference on Machine Learning and Cybernetics*. Piscataway NJ: IEEE, 2006.

[9] Mollineaux, M. G. et al. “Simulating the dynamics of wind turbine blades: Part I, model development and verification”. In: *Wind Energy* 16.5 (2013), pp. 694–710.

[10] Wang, X., Lin, S., and Wang, S. “Dynamic Friction Parameter Identification Method with LuGre Model for Direct-Drive Rotary Torque Motor”. In: *Mathematical Problems in Engineering* 2016 (2016), pp. 1–8.

[11] Wenjing, Z. “Parameter Identification of LuGre Friction Model in Servo System Based on Improved Particle Swarm Optimization Algorithm”. In: (2007), pp. 135–139.

[12] Higdon, D. et al. “Computer Model Calibration Using High-Dimensional Output”. In: *Journal of the American Statistical Association* 103.482 (2008), pp. 570–583.

[13] Gehb, C. M. “Uncertainty evaluation of semi-active load redistribution in a mechanical load-bearing structure”. Dissertation. Darmstadt: Technische Universität Darmstadt, 2019.

[14] Atamturktur, S., Hemez, F. M., and Laman, J. A. “Uncertainty quantification in model verification and validation as applied to large scale historic masonry monuments”. In: *Engineering Structures* 43 (2012), pp. 221–234.

[15] van Buren, K. L. et al. “Simulating the dynamics of wind turbine blades: Part II, model validation and uncertainty quantification”. In: *Wind Energy* 16.5 (2013), pp. 741–758.

[16] Gehb, C. M. et al. “Bayesian inference based parameter calibration of the LuGre-friction model”. In: *Experimental Techniques* (2019), in press.

[17] Enss, G. C. et al. “Device for optimal load transmission and load distribution in lightweight structures (Kraftübertragungsvorrichtung)”. DE 10 2014 106 858 A1.

[18] Mallapur, S. and Platz, R. “Quantification and Evaluation of Uncertainty in the Mathematical Modelling of a Suspension Strut Using Bayesian Model Validation Approach”. In: *Model Validation and Uncertainty Quantification, Volume 3*. Ed. by Barthorpe Robert J. et al. Conference proceedings of the Society for Experimental Mechanics series. Cham: Springer International Publishing, 2017, pp. 113–124.

[19] Kuypers, F. *Klassische Mechanik*. Wiley, 2016.

[20] Do, N. B., Ferri, A. A., and Bauchau, O. A. “Efficient Simulation of a Dynamic System with LuGre Friction”. In: *Journal of Computational and Nonlinear Dynamics* 2.4 (2007), p. 281.

[21] Götz, B. “Evaluation of uncertainty in the vibration attenuation with shunted piezoelectric transducers integrated in a beam-column support”. Dissertation. Darmstadt: Technische Universität Darmstadt, 2018.

[22] Schaeffner, M. “Quantification and evaluation of uncertainty in active buckling control of a beam-column subject to dynamic axial loads”. Dissertation. Darmstadt: Technische Universität Darmstadt, 2019.

[23] Markert, R. *Strukturdynamik*. Mechanik. Aachen: Shaker, 2013.

[24] Trucano, T. G. et al. “Calibration, validation, and sensitivity analysis: What’s what”. In: *Reliability Engineering & System Safety* 91.10-11 (2006), pp. 1331–1357.

[25] Saltelli, A. *Global sensitivity analysis: The primer*. Chichester, England and Hoboken, NJ: John Wiley, 2008.

[26] Dodge, Y., ed. *The concise encyclopedia of statistics*. [Updated ed.] Springer reference. New York, NY: Springer, 2010.

[27] Nagel, J. B. “Bayesian techniques for inverse uncertainty quantification”. Dissertation. Zürich: ETH Zürich, 2017.

[28] Smith, R. C. *Uncertainty quantification: Theory, implementation, and applications*. Vol. 12. Computational science & engineering. Philadelphia, Pa.: Soc. for Industrial and Applied Mathematics, 2014.

[29] Kennedy, M. C. and O’Hagan, A. “Bayesian calibration of computer models”. In: *Journal of the Royal Statistical Society: Series B (Statistical Methodology)* 63.3 (2001), pp. 425–464.

[30] Bayes, T. “An essay towards solving a problem in the doctrine of chances. By the late Rev. Mr. Bayes, F. R. S. communicated by Mr. Price, in a letter to John Canton, A. M. F. R. S”. In: *Philosophical Transactions of the Royal Society of London* 53 (1763), pp. 370–418.

[31] Matthew Riddle and Ralph T. Muehleisen. “A Guide to Bayesian Calibration of Building Energy Models”. In: *ASHRAE/IBPSA-USA*. 2014.